



Study of the Self-starting Performance of a Vertical-axis Wind Turbine

Z. Xu^{1†}, X. Dong¹, K. Li¹, Q. Zhou² and Y. Zhao¹

¹ College of Mechanical Engineering, Zhejiang University of Technology, Hangzhou, Zhejiang Province, 310014, PR China

² College of Computer Science and Technology, Zhejiang University of Technology, Hangzhou, Zhejiang Province, 310014, PR China

†Corresponding Author Email: xzzym@zjut.edu.cn

ABSTRACT

The self-starting performance of vertical-axis wind turbines (VAWTs) is crucial for their widespread utilization. Conventional evaluation methods using the static torque coefficient (CTS) or self-starting time have limitations. "The minimum 1st derivative of angular acceleration in the lift acceleration state" is proposed to serve as a suitable indicator for the completion of self-starting. Understanding the behavior of the self-starting process in VAWTs is crucial for optimizing power output. A comprehensive methodology is used that integrates experiments and computational fluid dynamics (CFD). Wind tunnel experiments are conducted to evaluate the self-starting and power output performance of the turbines. CFD is employed utilizing the Fluent 6DOF module to investigate the torque and flow field characteristics during the self-starting process. Additionally, the objectives of our study are to investigate the effect of static evaluation methods on the dynamic start-up process and to explore the effects of airfoil type, pitch angle, and inlet wind speed on the self-starting behavior of turbines. The results indicate that a high CTS ensures initial rotation, but the subsequent self-starting time remains independent of this factor. Increasing the pitch angle enhances the self-starting performance. At an inlet speed of 5 m/s, for the NACA2418 airfoil turbine, the self-starting times for pitch angles of 10° and 5° are reduced by 20% and 12%, respectively, compared to that for 0°. The NACA0018 airfoil turbines with pitch angles of 0° and 5° fail to complete self-starting. The airfoil type also plays a crucial role, with the NACA2418 airfoil demonstrating superior self-starting performance and power performance. Furthermore, the minimum self-starting wind speed of the NACA0018 airfoil turbine was explored and determined to be between 5.5 m/s and 6 m/s. The utilization of this novel self-starting evaluation method addresses the limitations of traditional approaches, providing a more universally applicable interpretation of the characteristics of turbine self-starting behavior.

Article History

Received September 6, 2023

Revised January 5, 2023

Accepted January 16, 2024

Available online March 27, 2024

Keywords:

Vertical-axis wind turbine

Self-starting performance

Evaluation method

Wind tunnel experiment

Transient numerical simulation

1. INTRODUCTION

As countries worldwide aim to be carbon neutral, clean energy such as wind power will account for an increasing share of energy. According to the GWEC, an additional 1,221 gigawatts (GW) of new capacity is projected to be installed by 2030 (GWEC, 2023). This includes the development of horizontal axis wind turbines in the direction of enhanced power generation on land and sea (Kaya et al., 2018). For urban areas, the demand for distributed energy installation has further increased, and its development has been rapid in recent years. Small VAWTs are receiving increasing amounts of attention (Tong, 2010; Alam & Golde, 2013; Battisti et al., 2018;

Twidell, 2021). VAWTs have the advantages of simple structures, no wind yaw devices, transmission mechanisms located on the ground, easy maintenance, low noise, and increased suitability for urban environments (Islam et al., 2013; Rezaeiha et al., 2018a; Su et al., 2019). VAWTs encompass both Savonius rotors and Darrieus rotors in their classification. (Hand & Cashman, 2020). The Darrieus rotor has a higher C_p than the Savonius rotor (Sheldahl et al., 1978; Chang et al., 2021). The Darrieus rotor generates low or even negative torques at azimuthal angles; due to the inherent characteristics of the Darrieus rotor, its blades perform little or no work at a low tip speed ratio (TSR) (Arab et al., 2017). The inherent poor start-up capability is a crucial factor limiting its

application (Worasinchai et al., 2016).

Research into the self-starting capabilities of VAWTs has been a widely explored topic. To improve the self-starting capabilities of these materials, many scholars have put forth a series of methods: blade airfoils (various airfoils (Hashem & Mohamed, 2018) and blades with GFs (Zhu et al., 2021)), turbine parameters [solidity (Li et al., 2016; Bangga et al., 2021), pitch angle (Su et al., 2020), aspect ratio (Li et al., 2017), J-shaped airfoil blades (Celik et al., 2022)], auxiliary device addition [wind gathering devices (Li et al., 2020), flat plate deflectors (Wong et al., 2018)] and Darrieus rotors with drag-driven Savonius rotors (Kumar et al., 2018)].

The researchers have adopted different definitions of self-starting performance literature for VAWTs. Ebert and Wood (1997) believed that there was available power to generate and complete self-starting during the process. This definition of "available power" is not accurate. When the turbine has a lower TSR, the turbine can generate very little torque to generate electricity, and the turbine does not reach the optimal power point. Lunt (2005) proposed that the self-start was completed when only the turbine accelerated from a static to the final stable state and when the blade tip velocity exceeded the wind speed. It means TSR is greater than 1. Celik et al. (2022) and Asr et al. (2016) reported that when the $TSR \geq 1$, the turbine was in a stable state, did not enter the lift acceleration state, and did not reach the appropriate power output point. Celik et al. (2020) and Sun et al. (2020) consider the transition of the turbine from a stationary state to stable rotation as indicative of successful self-starting. Additionally, they employ time as a key metric for evaluation. According to this statement, when the turbine rotates at high speed, fluctuations in the turbine will be more frequent, which is a challenge to the fatigue characteristics of itself (Liu et al., 2019). The turbine usually generates the maximum torque value in the lift acceleration state and power output in this state. (Worasinchai et al., 2016) suggested that self-start was achievable as long as thrust was consistently generated along the Darrieus flight path. Their approach was grounded in proposing an analogy between the physical description of the Darrieus turbine starting capability and the pitch-heave concept observed in the flapping mechanisms of animals. While the definition is clear, the method's complexity poses challenges for practical application, causing difficulty to analogize each type of VAWTs to flapping mechanisms of birds. Consequently, this approach lacks practical applicability on a broad scale. Bhuyan and Biswas (2014), Singh et al. (2015), Arpino et al. (2018), Mohamed et al. (2019), Mohamed et al. (2020), Su et al., (2020) and Al-Obaidi and Qubian (2022), assessed the ability to self-start by measuring the turbine's static torque at different initial azimuthal angles. For this definition, the static torque only described the static state and could not sufficiently describe the actual self-starting process. In some cases, the turbine could rotate; however, the TSR was at a low level, the turbine could not enter the lift acceleration state, and the turbine could not output power. Although these definitions have certain truths, there are many limitations. In conclusion, methods for evaluating self-starting performance can be categorized into two types: static start-up performance and dynamic start-up performance. Static start-up performance refers to the static torque at the initial azimuthal angle. Dynamic start-up performance

refers to the time it takes for the wind turbine to transition from static rotation to a specific TSR.

For the self-starting process, (Hill et al., 2008) divided it into four parts: the "linear regime" state, "plateau" state, "lift" state, and "equilibrium" state. The turbine generates almost no torque in the "plateau" state. This area (Baker, 1983) is described as a dead zone. In this state, the torque coefficient reaches its minimum value. The turbine can be easily and quickly stopped when loading. Worasinchai et al. (2012) divided the start-up process into a "combined state" and a "full lift-driven state". Within the "full lift-driven state," it was divided into two thrust generation states: "discrete" and "continuous". They found that the turbine could be locked in the deadband when generating discontinuous thrust. The "continuous thrust-producing" state coincided with Hill's description of "lift" and "equilibrium". Most VAWTs are in the "lift" state for the power output.

The self-starting performance of VAWTs limits its widespread development. Based on the above scholars' investigations of self-starting process and performance evaluation methods, none of the existing studies have explored the turbines' self-starting behavior while considering angular acceleration data. In this study, a novel approach for evaluating self-starting performance is introduced for the first time. The turbine rotation to the "the minimum 1st derivative of angular acceleration in the lift acceleration state" is used as the completion of the self-starting process evaluation. The self-starting characteristics of lift-driven turbines is investigated by experiments and CFD. Following sensitivity studies to ensure the accuracy of the CFD model, a comprehensive comparison of the output results with experiment was conducted. Subsequently, a comprehensive examination of the self-start process of the wind Turbine was conducted. The impact of static torque at different initial azimuthal angles on the self-start process was examined. Additionally, the causes of differences between the airfoils and pitch angles under the inlet wind speed at 5m/s during the self-starting process were investigated. The contributions of lift and drag to torque are analyzed within critical regions. Furthermore, the minimum self-starting wind speed was explored, and the factors that contribute to the success or failure of the self-starting mechanism were examined.

2. EXPERIMENTAL SETUP

The experiments were conducted in the wind tunnel laboratory at Zhejiang University of Technology. The wind tunnel structure consists of an air inlet, a contraction, a test, a diffuser, and fan sections, as shown in Fig. 1. The length of the wind tunnel is 13.85 m. The tunnel is driven by a six-blade fan. The test section is closed, with dimensions of 2 m long, 1.2 m wide, and 1.2 m high. Two-speed measurement systems are used for the differential pressure and hot wire anemometer. In the test section, the wind speed range is 3 m/s to 10 m/s, with a measurement accuracy of $\pm 3\%$, and the turbulence intensity is maintained below 0.5%.

The entire wind turbine experimental setup is illustrated in Fig. 2 and primarily consist of airfoil blades, a support frame, a main shaft, and a magnetic powder dynamometer. The airfoil blades are designed and

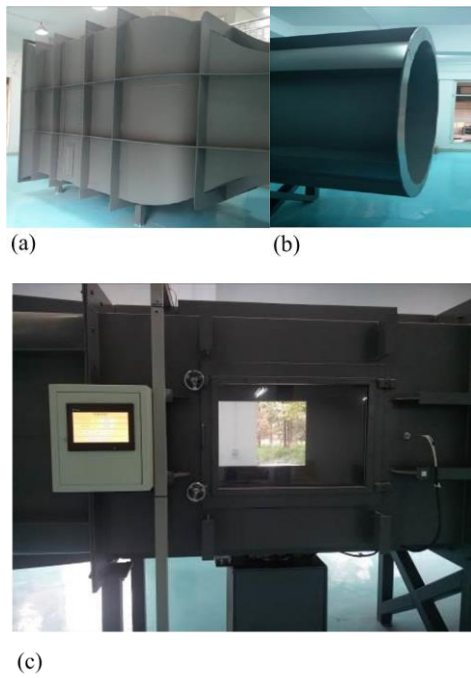


Fig. 1 Wind tunnel used in this experiment: Inlet and contraction section (a), outlet section (b), and test section (c)

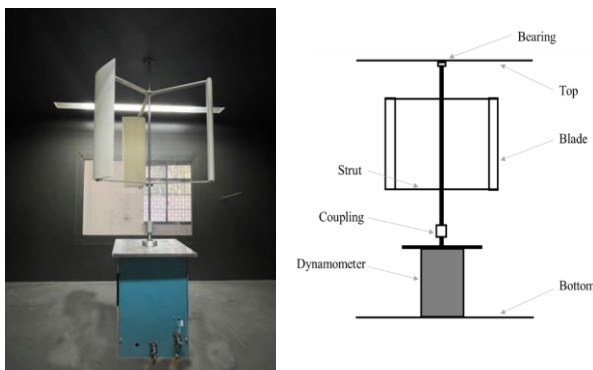


Fig. 2 Wind turbine experimental device

manufactured using three-dimensional printing technology, employing ABS-like stereoscopic light modeling resin as the material. According to the information provided by the three-dimensional printing supplier, they utilized an SLA three-dimensional printer with a layer height set at 25 micrometers. The achieved surface roughness can reach less than 20 micrometers. The support frame is made of aluminum alloy, and there is a radial groove at the connection of the blade to adjust the pitch angle. The main shaft is made of chrome-plated high-carbon steel; the lower end of the rotating shaft of the turbine is connected with a magnetic powder dynamometer (model: JC5288, torque range: 10 N · m, precision: 0.1% FS, maximum rotational speed: 1500 r/min, rotation accuracy: 1 r/min). Magnetic powder dynamometers are used to measure the rotational speed, torque, and power output. Table 1 outlines the features of the wind turbine. Figure 3 shows the relative rotation of the blades.

The static start-up performance test is designed to determine the static torque at various azimuthal angles.

Table 1 features of the wind turbine used in the experiment

Parameter	Symbol	Value
Blade profiles	-	NACA0018, NACA2418, NACA4418
Pitch angle	β	0°, 5°, 10°
Blade chord	C	133.33 mm
Number of blades	N	3
Rotor height	H	400 mm
Diameter	D	500 mm
Solidity	σ	0.8
Moment of inertia	I	0.066 kgm ²

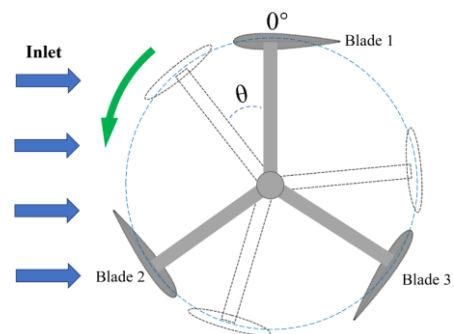


Fig. 3 Relative rotation of the turbine blades

The wind tunnel fan is initiated in the experiment, and a waiting period of 30 s follows until the flow field within the wind tunnel achieves essential stability. Afterward, the average torque data for the specific azimuth angle are recorded over a 30 s interval. The dynamic start-up performance test is executed to analyze the wind turbine response when the TSR fluctuates from 0 to its maximum stable value at a defined wind speed. In this experimental setup, a magnetic powder dynamometer applies a predetermined excitation current to prevent the wind turbine from initiating rotation. Subsequent to ensuring the stability of the flow field in the wind tunnel, the excitation current is then reduced to zero, initiating the rotation of the turbine. The torque-speed sensor integrated into the magnetic powder dynamometer simultaneously records the changes in torque and rotational speed over time. The power performance under various TSR conditions is measured by adjusting the excitation current to induce changes in the turbine's rotational speed. Wind turbines have the following important parameters: power coefficient C_p , tip speed ratio TSR, torque coefficient C_t , static torque coefficient CTS, and angular acceleration α . C_p is the dimensionless coefficient of power. The TSR is a dimensionless parameter that signifies the ratio between the rotational speed of the blade and the speed of the free-flowing air. C_t and CTS are the dimensionless coefficients of torque and static torque, respectively. C_t and CTS serve as valuable metrics for reporting the performance of a turbine. α is the rate of change in angular velocity with respect to time.

$$C_p = \frac{n\pi T}{15\rho AU^3} \quad (1)$$

$$TSR = \frac{n\pi R}{30U} \quad (2)$$

$$Ct = \frac{2T}{\rho ARU^2} \quad (3)$$

$$CTS = \frac{2T_s}{\rho ARU^2} \quad (4)$$

$$\alpha = \frac{d\omega}{dt} = \frac{\omega_{i+1} - \omega_i}{t_{i+1} - t_i} \quad (5)$$

where ρ (kg/m^3) represents the air density, A (m^2) represents the swept area, U represents the wind speed, T (Nm) represents the dynamic torque, n (rpm) represents the rotation speed, T_s (Nm) represents the static torque, ω (rad/s) represents the angular velocity, and t represents the time.

Furthermore, the blockage ratio (Roy & Saha, 2014) is the ratio of the cross-sectional area of the turbine structure to the cross-sectional area of the wind tunnel. The value is 3.47% in our experiment. All data were adjusted accordingly (Howell et al., 2010; Al-Obaidi, 2018).

3. NUMERICAL MODELING AND SENSITIVITY STUDIES

3.1 Model Geometry and Computational Domain

In this study, a two-dimensional model is used for CFD. The three-dimensional model of the experimental rotor is simplified into a two-dimensional model. The testing equipment of the turbine is mainly composed of airfoil blades, a rotating shaft, a support frame, a transmission device, and a control circuit. Since the wind wheel, which consists of blades, is the only part that converts wind energy into mechanical energy, the rest of the wheel can be disregarded, leaving only blades and shafts. The three-dimensional model of the wind turbine can be simplified into a two-dimensional model. Many scholars have verified that two-dimensional CFD is sufficient to accurately investigate the self-start characteristics of VAWTs (Sobhani et al., 2017; Li et al., 2019). In the experiment, the moment of inertia(I) was 0.066 kgm^2 whereas in the two-dimensional CFD simulation, the I was recalculated to account for a turbine height of 1000 mm instead of the 400 mm used in the experiment. The recalculated inertia value in the simulation was determined to be 0.165 kgm^2 (Zhu et al., 2015).

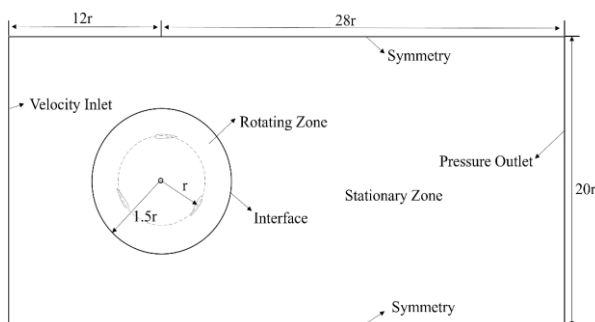


Fig. 4 Computational domain and boundary conditions

An appropriate computational domain size is essential for obtaining numerical simulation results. Figure 4 shows the computational domain, which is divided into two parts: a circular rotating region and a rectangular stationary region, where r represents that the radius of the wind turbine is 250 mm. The computational domain's top and bottom boundaries are Symmetrical (Nobile et al., 2014; Al-Obaidi et al., 2023b). The rotational center of the turbine is positioned $12r$ from the inlet and $28r$ from the outlet. A sufficiently large domain can allow for better capturing of the overall characteristics of the wind turbine, and the wake is fully developed (Almohammadi et al., 2013; Nobile et al., 2014; Rezaeiha et al., 2018b; Al-Obaidi, 2023b; Al-Obaidi & Alhamid, 2023).

3.2 Boundary Conditions and Computational Methods

The velocity inlet boundary is established along the left side of the rectangular area. On the right side, the boundary is defined as the pressure outlet. The top and bottom sides are subjected to wall conditions, and the blade surface inside the circular area is set as a nonslip wall boundary. The SST $k-\omega$ model integrates the advantages of the $k-\omega$ and standard $k-\epsilon$ models by employing the $k-\omega$ model in the boundary layer and transitioning to standard $k-\epsilon$ behavior in the free stream; this model aims to enhance accuracy and general applicability in turbulent flow simulations. Due to its favorable agreement with experimental results, the SST $k-\omega$ model is currently a prevalent choice in numerous CFD simulations (Asr et al., 2016; Al-Obaidi, 2019; Mohamed et al., 2019; Celik et al., 2022; Al-Obaidi, 2023a) and is suitable for this study. In this research, the fluctuation in the turbine's rotational speed, propelled by the wind, is computed by assessing the torque generated by the blades during each time step. The circular rotating region is a dynamic mesh zone. In the dynamic mesh zone, the 6DOF solver is used to determine one rotational degree of freedom, the rotational center, and the I. When the incident wind interacts with the blades, the 6DOF solver calculates the external forces and torques exerted. This computation enables the rotation of the rotor in response to the applied forces. Moreover, the dynamic mesh zone rotates (Asr et al., 2016; Maalouly et al., 2022).

3.3 Meshing and Sensitivity Study

The process of mesh generation is a crucial aspect of CFD simulations, significantly influencing their accuracy. ANSYS recommends that at least 10 element boundary layers should be used for the blade boundary layer to ensure accurate modeling (Ansys, 2018). In this study, the mesh consisted of 15 layers of elements. The height of the first cell around the blade was set to $3 \times 10^{-5} \text{ m}$, and the growth rate with a growth rate of 1.1 near the blade boundary. Beyond the inflation region, unstructured grids are employed in both the rotating and static regions to accommodate the intricate and variable geometric shapes of the blades. Compared with structured grids, unstructured grids provide greater flexibility and accuracy in accurately representing complicated geometric shapes. Considering that the flow field around the blades is very complex when the turbine is running, the grids near the airfoil blades are encrypted to enhance the precision of the numerical simulation results. The mesh is shown in Fig. 5

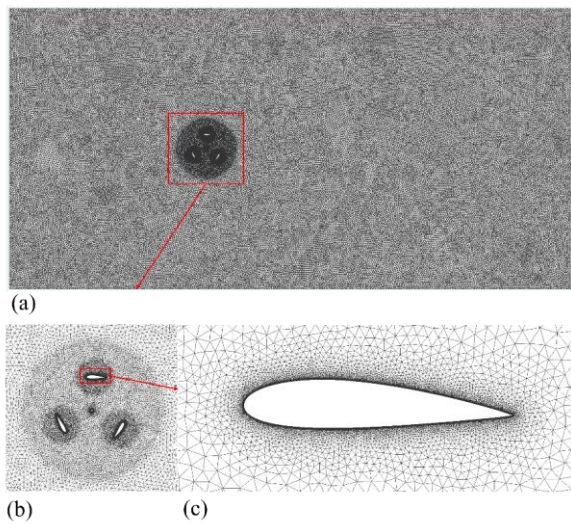


Fig. 5 Grid details for the whole domain (a), the rotating domain (b), and the blade (c)

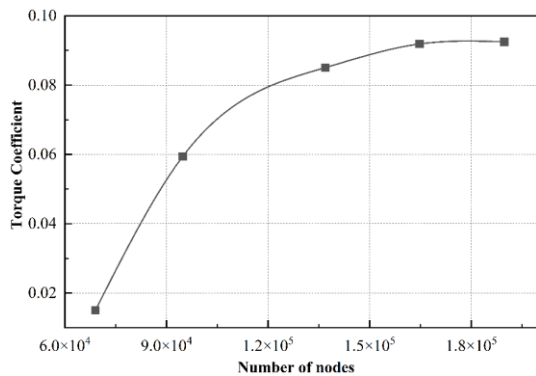


Fig. 6. Torque coefficients for different numbers of nodes

Increasing the number of nodes in the computational domain can yield more accurate results. However, as the number of nodes increases, both the computational load and the required processing time simultaneously increase. (Balduzzi et al., 2016; Al-Obaidi et al., 2023a). To determine the optimal number of nodes, a grid sensitivity

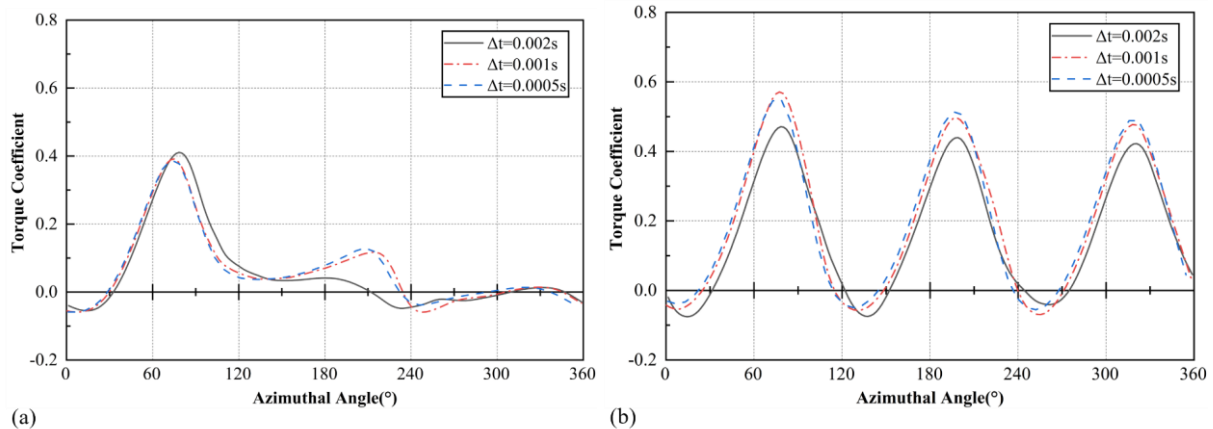


Fig. 7 Torque coefficient as a function of the azimuthal angle for the time step size at the 15th circle: the single blade (a) and the turbine (b)

study was conducted to ensure that, changes in the number of nodes within a specific range of node counts have minimal impact on the results. In the present work, five different numbers of nodes are used by changing the node size on the blade and around the rotating region. The respective torque values are calculated under the simulation conditions of a TSR of 1.3. The five grid numbers are 69037, 94816, 136918, 164715, and 189472. The torques calculated under the five conditions are shown in Fig. 6. Evidently, within the range of 130,000 to 180,000 nodes, the torque coefficient remains relatively unaffected by variations in the number of nodes. Considering the calculation efficiency, approximately 160,000 nodes were selected for this study.

3.4 Time Step Size Study

To validate the significance of the time step in determining the outcomes, the results for three time step sizes are verified, namely, $\Delta t_1 = 0.002$ s, $\Delta t_2 = 0.001$ s, and $\Delta t_3 = 0.0005$ s. Fig. 7 shows that the wind turbine rotates for the 15th circle, changes in the C_t of a single blade and the turbine can be observed. There is only a slight difference between Δt_2 and Δt_3 , and C_t tends to be the same. Therefore, $\Delta t_2 = 0.001$ s is selected for further simulation to reduce the calculation time. Compared with previous studies, the time step is slightly larger. In recent studies (Asr et al., 2016), when the TSR was 4 or greater under stable condition, and the rotational speed was higher than that of the turbine model in this paper, and a minor time step was used.

4. RESULTS AND DISCUSSION

4.1 Numerical Simulation Validation Against Experimental Data

Figure 8 shows the NACA2418 turbine experiment and numerical simulation of the self-starting process. The turbine takes approximately 130 s to accelerate from a static state to a stable condition ($I = 0.066$ kgm^2). The numerical simulation takes approximately 73 s ($I = 0.165$ kgm^2). To facilitate the comparison between the experiment and numerical simulation, a nondimensional time axis is established as t/T , where T represents the time at which the stable condition is achieved. The time gap between the experiment and the CFD mainly occurs

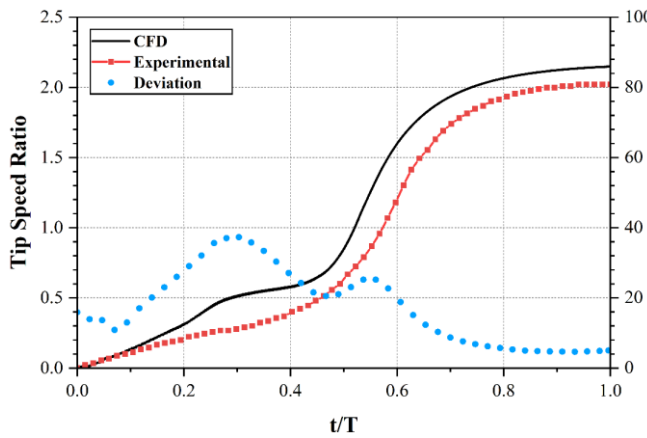
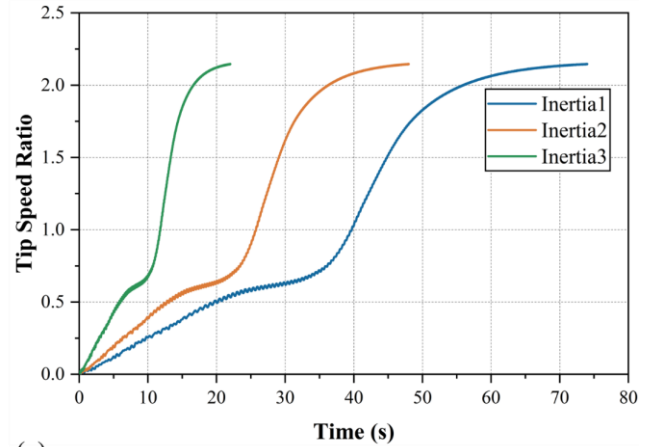


Fig. 8 Variation in the TSR with the normalized time for comparing the present two-dimensional CFD and experimental results

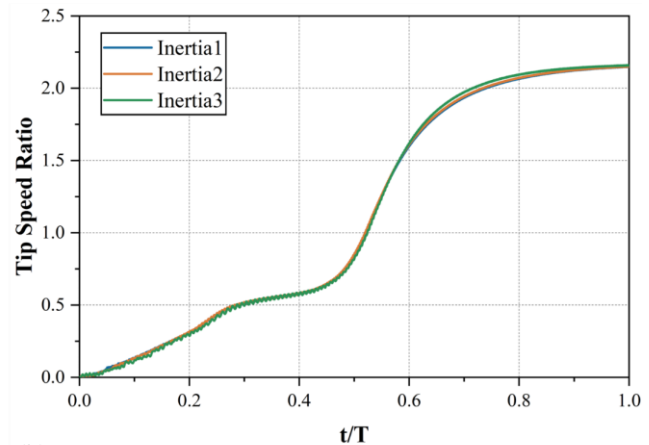
because the resistance of the magnetic particle dynamometer is disregarded in the numerical simulation and due to the blockage effects in the wind tunnel. When the $TSR < 1$, notable differences emerge between the experiment and CFD ($0.2 < t/T < 0.5$), mainly because the computational model is two-dimensional and has limitations in predicting complex flows around blades. Especially when the turbine has a low TSR, the three-dimensional dynamic stall is more complex than its two-dimensional counterpart owing to the presence of dynamic characteristics of the wind leading to stall on the blades. Subsequently, as the wind turbine enters the lift-driven state, the deviation diminishes. During the stable condition, the maximum deviation observed is approximately 5%. The experimental and numerical simulation results show a high level of agreement with minimal deviation.

In the wind tunnel experiment, the I is 0.066 kgm^2 . The I has a direct impact on the turbine's angular acceleration. Under the condition of generating the same aerodynamic torque, a smaller I correlates to a greater corresponding angular acceleration of the turbine and a quicker acceleration. [Celik et al. \(2020\)](#) studied the self-starting process of four moments of inertia of a turbine. They found that increasing the turbine's I extended the time needed to attain the stable condition. However, this change had a negligible impact on both the self-start and the ultimate speed achieved. In this study, to shorten the time consumed by numerical simulation without affecting the research on the dynamic start-up performance, an appropriate reduction is made to the I of subsequent turbines. Three turbines with different I are used, as follows: Inertia 1, 0.165 kgm^2 ; Inertia 2, 0.11 kgm^2 ; and Inertia 3, 0.055 kgm^2 . Figure 9(a) shows that reducing the turbine I from 0.165 kgm^2 to 0.055 kgm^2 results in a shortened time to reach its stable condition. Therefore, Fig. 9(b) illustrates the variation in the TSR over normalized time for the four inertia cases. Evidently, the TSRs of all I similarly increase, indicating that their dynamic start-up processes are basically the same. Therefore, the subsequent numerical simulation uses 0.55 kgm^2 to decrease the calculation time.

As shown in Fig. 10(a), based on insights into the self-starting process from [Worasinchai et al. \(2012\)](#) and



(a)



(b)

Fig. 9 Variation in the TSR with time (a) and normalized time (b) for different moments of inertia.

[Hill et al. \(2008\)](#), we apply their methods to the self-starting process in this study. [Worasinchai](#) divides the self-starting process into a "combined state" and a "full lift-driven state". Moreover, the "full lift-driven state" is further divided into two thrust generation states: "discrete" and "continuous". They considered reaching the "continuous thrust-producing state" to be the completion of the self-starting process, as indicated by the red dot in the figure. [Hill](#) divided the self-starting process into a "linear regime", "plateau" state, "lift" state, and "equilibrium" state. [Hill and Celik et al. \(2020\)](#) had the same perspective and considered the wind turbine reaching stable condition as the completion of the self-starting process, as indicated by the green dot in the figure. [Lunt \(2005\)](#), on the other hand, adopted a TSR of 1 as the self-starting point, as illustrated by the blue dot in the figure. As illustrated in Fig. 10(a), the turbine's angular acceleration is more significant than 0.5 rad/s^2 in the lift acceleration state. When $TSR = 1.302$, the maximum α is 1.15 rad/s^2 . The load is gradually increased in the stable condition of the turbine. In the right section of the peak α , the turbine slows down to a series of stable rotational speeds for power output. Figure 10(b) shows that $TSR = 1.292$ and the maximum $C_p = 0.146$; these matches where the maximum α occurs in the self-starting process. When the load increases to the left of the peak α (the first half of the lift acceleration state), the turbine can to a complete stop in a very short time. The load is greater than the torque-generating capacity of the turbine, resulting in the

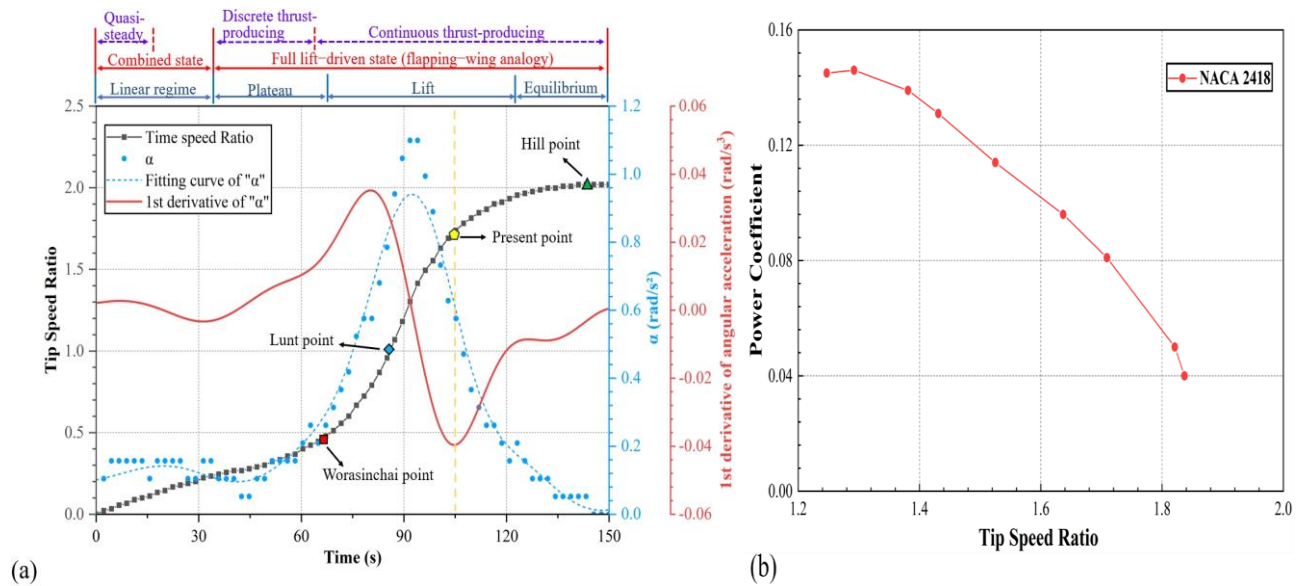


Fig. 10 NACA2418 turbine self-starting process (a) and power output (b)

turbine's self-starting failure. The 1st derivative of α is the rate of change in α , as shown in Fig. 10(a). Apparently, the 1st derivative of α in the lift acceleration state curve shows three important states in the lift acceleration state. When the 1st derivative of α increases to the peak value, the positive change rate of α is the largest. The turbine will accelerate toward the optimal power coefficient point. For the 1st derivative of $\alpha = 0$, α increases to the maximum. The turbine reaches the vicinity of the optimum power coefficient point with a TSR of approximately 1.3. Finally, the 1st derivative of the angular acceleration decreases to the minimum value. Thus, the negative change rate of α is the largest, which corresponds to the second half of the lift acceleration state, after which the turbine will slowly reach stable condition. Under stable condition, fluctuations in the turbine will occur more frequently, posing a challenge to the fatigue characteristics of the turbine itself. The turbine is at the highest speed. Therefore, the turbine enters "the minimum 1st derivative of angular acceleration in the lift acceleration state" as the mark of completion of self-starting. Figure 10(a) illustrates that the turbine takes 105 s to complete self-starting.

4.2 Effect of Static Torque at Different Initial Azimuthal Angles on the Dynamic Start-up Process

Figure 11 presents the curve of the CTS of the NACA2418 airfoil turbine with a 0° pitch angle in the experiment and numerical simulation. Considering that one period of the CTS of the three-blade turbine is 120° , only the CTS of the azimuthal angles from 0° to 120° is shown. The experiment and numerical simulation show the same trend. According to the numerical simulation, the maximum CTS reached 0.0423 at 80° , which was 3.7 times greater than the minimum CTS of 0.0114 at 10° . In the experiment, the influence of the initial azimuthal angle on the dynamic start-up process is studied. Due to the resistance of the turbine and the dynamometer equipment, the turbine does not rotate or wobble and then enters the static state at the beginning of some initial azimuthal angles with a small CTS. Based on the static torque at different azimuthal angles, a numerical simulation was

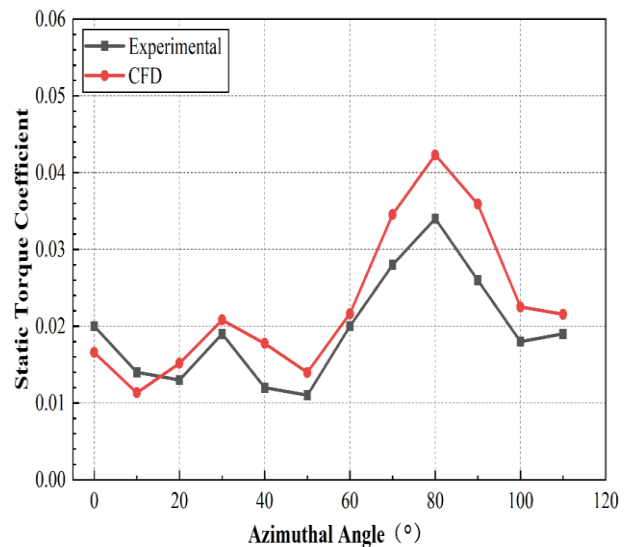


Fig. 11 Relationship between static torque coefficient and azimuthal angle

conducted to investigate the self-starting process for two initial azimuthal angles: a maximum CTS initial azimuthal angle of 80° and a minimum of 10° . The Fig. 12 shows that when the two initial azimuthal angles are rotated 1° , the maximum dynamic torque is generated at 80° , and the minimum is generated at 10° , which corresponds well with its CTS. Within 0.1 s, the angular velocity at an initial azimuth angle of 10° is lower than that at an initial azimuth angle of 80° , which further verifies that the CTS at 80° is greater than that at 10° . As shown in Fig. 13, when the time scale is increased to 12 s, the initial azimuthal angle of 10° first reaches the plateau state, and then the initial azimuthal angle of 80° takes 7s. At the same time, the initial azimuthal angle of 80° takes 9 s to reach the plateau state. An initial azimuth angle with a large static torque does not shorten the time needed to reach the plateau. Even at the 80° initial azimuthal angle with a large CTS, the time to reach the plateau is longer. This does not effectively describe that large CTS correlates to good self-starting performance.

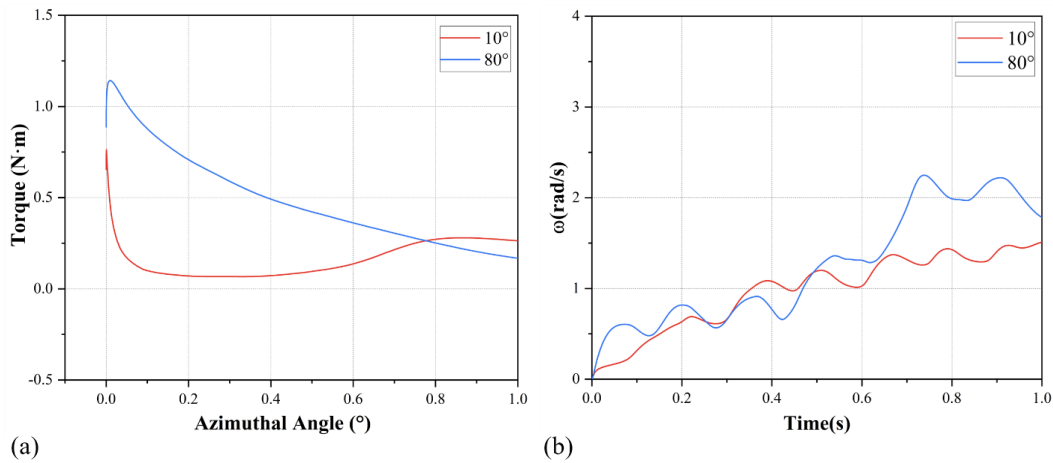


Fig. 12 Torque within a rotation of 1° (a) and angular velocity within a process of 0.1 s (b)

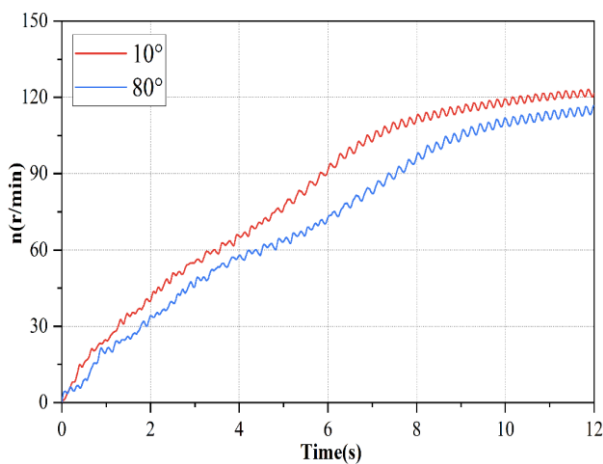


Fig. 13 Initial azimuthal angle 10° and initial azimuthal angle 80° dynamic start-up process

4.3 Effect of Pitch Angle on Dynamic Start-up Performance

Figure 14 shows the self-starting process of the NACA2418 turbines with three pitch angles. Evidently, as the pitch angle increases, the turbine speeds less time to complete self-starting; however, the time to approach the maximum TSR is increased. In comparison to the experimental results, the pitch angles of 0° and 5° in the experiment and 0° in the simulation exhibit a more apparent plateau state. Figure 15 shows the angular acceleration and 1st derivative of the angular acceleration curves of the self-starting process. It takes 84 s to complete the self-starting at a 10° pitch angle and 105 s at a 0° pitch angle. The self-starting time for a 10° pitch angle is 20% less than that for a 0° pitch angle. Although the self-starting time of the 10° pitch angle is short, its α is the lowest compared with those of the other two pitch angles. Figure 14(c) shows the deviation between the experiment and numerical simulation for three pitch angles. At $t/T < 0.4$, a significant deviation is observed due to extra contributors to resistive torque, specifically bearing frictional resistance and inherent resistance in magnetic powder dynamometers; this can potentially lead to an overestimation of the CFD results relative to the experiment.

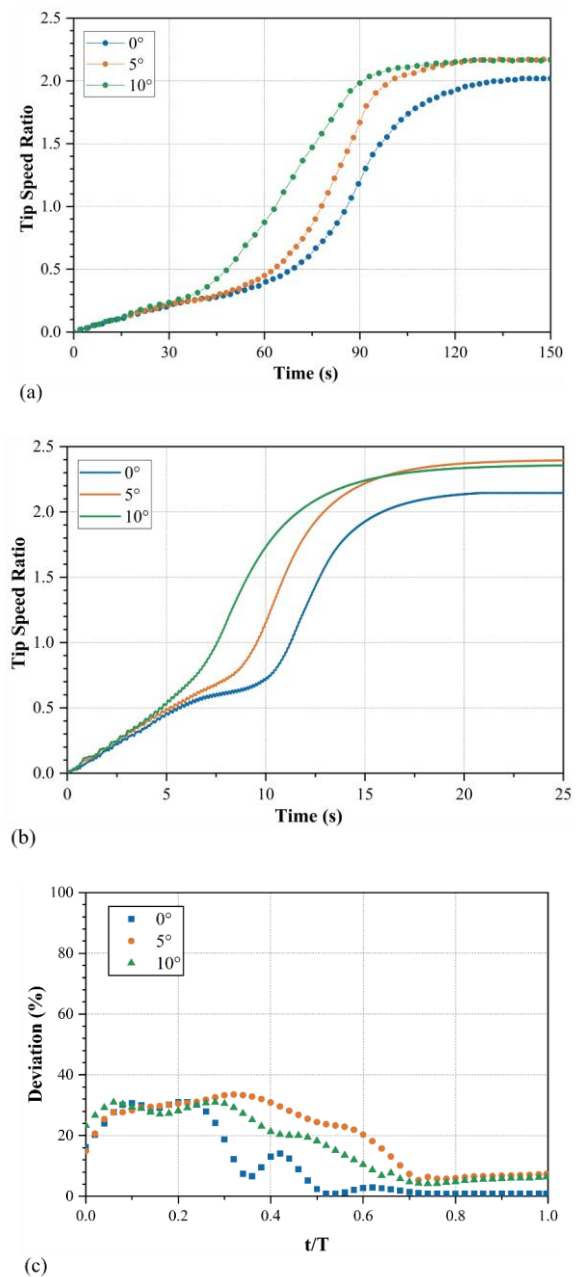


Fig. 14 NACA2418 turbine self-starting process: experiment (a), numerical simulation (b) and deviation (c)

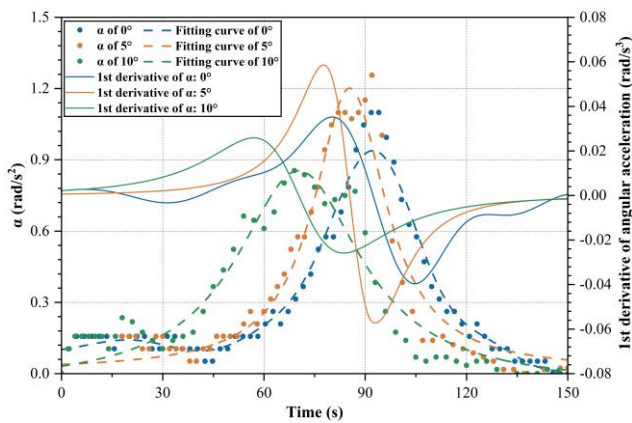


Fig. 15 Variation of the 1st derivative of the angular acceleration at pitch angles of 0°, 5° and 10° in the self-starting process

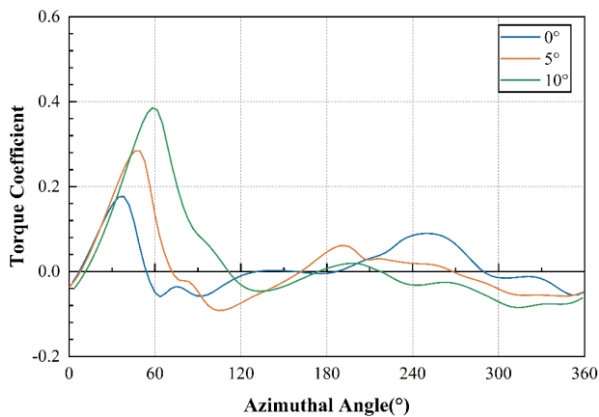
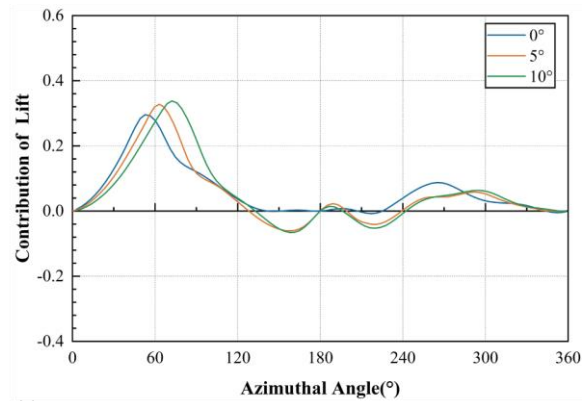


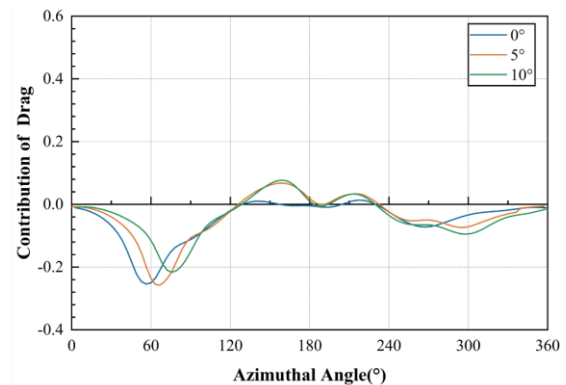
Fig. 16 Variation in the instantaneous torque coefficient of the single blade with the azimuthal angle for different pitch angles at a TSR = 0.6

Figure 16 shows the torque coefficient curve of the single blade at pitch angles of 0°, 5°, and 10° when TSR = 0.6 for numerical simulation. Under a pitch angle of 10°, the blade generates the maximum Ct at azimuthal angles ranging from 0° to 120°, improving the acceleration more than at other pitch angles. Figure 17 shows the contributions of the lift and drag forces to torque generation. The positive contribution of the lift at a 10° pitch angle to the torque is the largest when the azimuthal angle is less than 120°. In contrast, the difference between the contributions of lift at the other two pitch angles is minimal. However, in terms of the contribution of drag to torque, the absolute value of the negative torque contribution generated by resistance at a 10° pitch angle is the lowest. Minimal difference is observed between the other two pitch angles. Compared with the other two pitch angles, a pitch angle of 10° has a minor obstruction effect and slightly improves the torque.

Figure 18 shows the self-starting process of the NACA0018 airfoil turbine with pitch angles of 0°, 5°, and 10° in the simulation and experiment. First, the turbines with three different pitch angles can accelerate from stationary to rotational. However, the TSRs of turbines with pitch angles of 0° and 5° do not enter the lift acceleration state, and the turbines fail to exit the deadband. A turbine with a 0° pitch angle exhibits a low TSR of 0.18, whereas a turbine with a 5° pitch angle has a higher TSR, reaching 0.27. These turbines did not



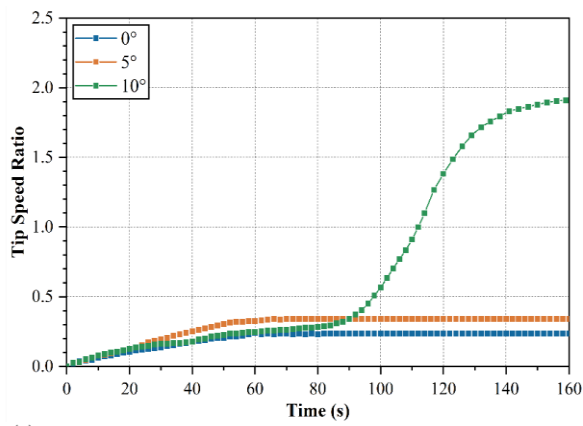
(a)



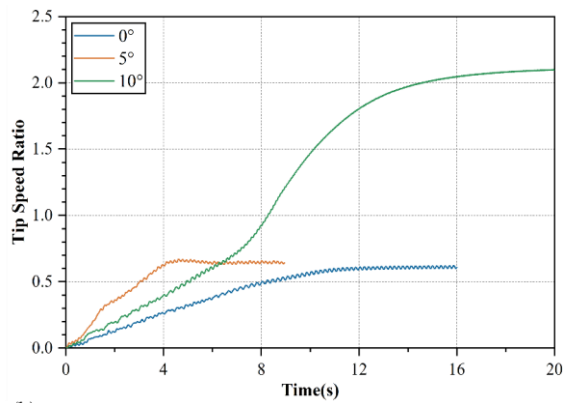
(b)

Fig. 17 Contribution of lift and drag to torque generation as a function of blade azimuthal angle for different pitch angles at a TSR = 0.6

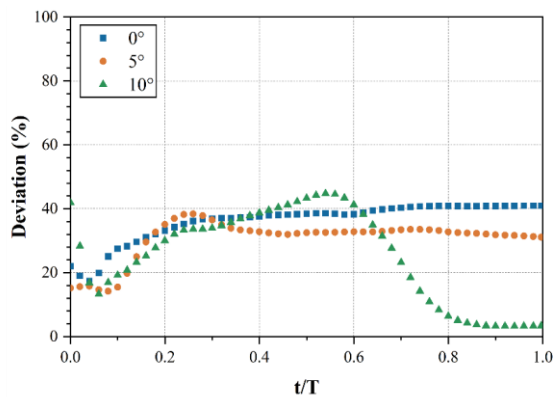
complete the self-starting process. In this case, although lift serves as the primary driving force for the turbine, the generated torque is too small to load for power output. Different from turbines with pitch angles of 0° and 5°, the turbine with a pitch angle of 10° still has an apparent acceleration trend after crossing the deadband and entering the second half of the lift drive state. Currently, the turbine completes its self-starting process and can load its power output. According to the simulation results, compared with a 0° pitch angle, a 5° pitch angle has a greater acceleration ability in the linear acceleration state. Nevertheless, they both do not complete the self-starting and remain in the deadband. At the final stable condition, the TSR at 5° is slightly greater than that at 0°, reaching approximately 0.69. A wind turbine with a pitch angle of 10° can enter the second half of the lift acceleration state and complete self-starting. The deviation curve in Fig. 18(c) illustrates a substantial discrepancy for the wind turbine that failed to self-start, while for the 10° pitch angle, successful self-starting occurred with minimal deviation, attributable to a delay in reaching the acceleration phase. Compared to the experiment, the numerical simulation disregards the natural resistance and generates more torque. The wind turbines that failed to self-start generate additional torque, leading to the maintenance of a higher TSR. The turbine that successfully completes self-starting can quickly pass through the plateau, enter the lift acceleration state, and complete self-starting. The final TSR reaches 2.1; this value has a small difference with the experimental TSR of 1.9. Despite disparities observed between the experiment



(a)



(b)



(c)

Fig. 18. NACA0018 turbine self-starting process: experiment (a) and numerical simulation (b) and deviation (c)

and simulation results, the self-starting process shows consistent correlation.

Figure 19 shows the variation in torque for a pitch angle of 0° at a maximum TSR = 0.6, 5° at a maximum TSR = 0.69, and 10° at a TSR = 0.7 in one rotation cycle. Turbines with pitch angles of 0° and 5° can generate stable torque and negative torque such that both working conditions are in a steady state. The positive C_t of the turbine with a pitch angle of 10° is the largest, while the absolute value of the negative C_t is the smallest compared with the other two pitch angles; these results demonstrate that the turbine is in the lift acceleration state.

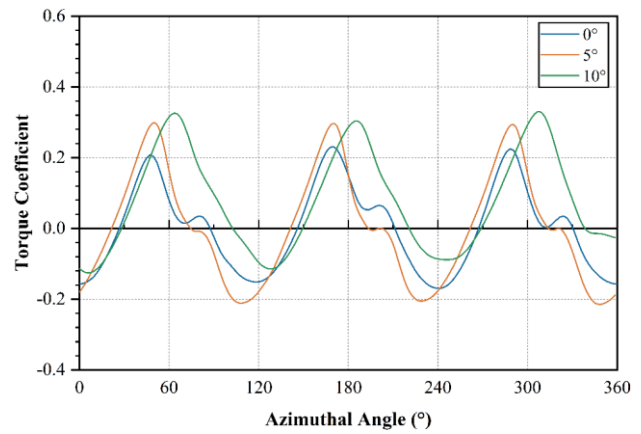


Fig. 19. Relationship between the torque coefficient and azimuthal angle for pitch angles of 0° at TSR = 0.6, 5° at TSR = 0.69, and 10° at TSR = 0.7

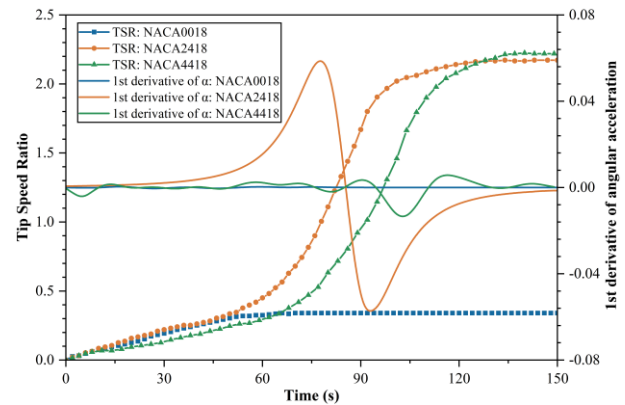


Fig. 20 Self-starting process of the NACAxx18 airfoil turbines

4.4 Effect of Different Airfoil Profiles on Dynamic Start-up Performance

Figure 20 shows the experiment's self-starting process for three NACAxx18 airfoil turbines with a 5° pitch angle. The NACA0018 airfoil turbine fails to complete self-starting. The NACA2418 airfoil turbine entered the second half of the lift acceleration state before the NACA4418 airfoil turbine completed its self-starting. The asymmetric NACA4418 airfoil with a greater relative camber could maintain a higher speed in the steady state. The NACA2418 airfoil turbine took 92 s to complete self-starting, while the NACA4418 airfoil turbine achieved self-starting in 104 s. Although the NACA0018 airfoil turbine failed to complete the self-starting process, when the experiment began, the initial speed (greater than the deadband speed) was used to assist the NACA0018 airfoil turbine in completing the self-starting such that it could carry out power output. The power coefficient of three NACAxx18 airfoil turbines as illustrated in Fig. 21, the NACA0018 symmetrical airfoil turbine had a higher C_p of 0.156; this value was 30% higher than that of the NACA4418 asymmetric airfoil turbine. The NACA4418 airfoil turbine exhibits minimal fluctuations in the 1st derivative of angular acceleration, indicating a lesser angular acceleration compared to the NACA2418 airfoil.

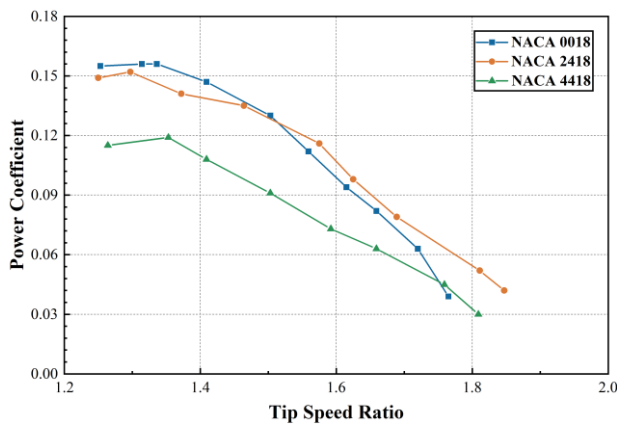


Fig. 21. Power coefficient comparison of the NACAxx18 airfoil turbines

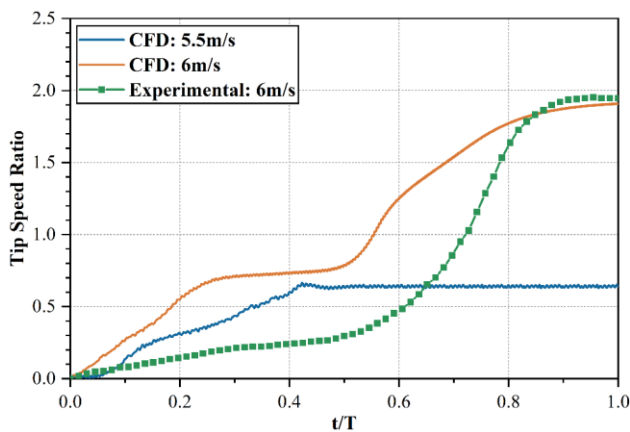


Fig. 22. Self-starting process at different inlet wind speeds: experiment and numerical simulation

This phenomenon also implies a weaker performance in terms of power generation. In general, the NACA2418 airfoil turbine had a stronger self-starting ability, but its C_p was lower than that of the NACA0018 airfoil, and its comprehensive performance was the best.

4.5 Study on the Minimum Self-starting Wind Speed

The symmetrical airfoil NACA0018 turbine with a 0°

pitch angle is investigated to study the minimum self-starting wind speed. According to the experimental and simulation results in Fig. 18, the NACA0018 airfoil turbine fails to self-start under 5 m/s condition.

Figure 22 shows the self-starting process of the experiment and the numerical simulation of different inlet wind speeds. In the experiment, the turbine can enter the second half of the lift acceleration state at 6 m/s, complete its self-start, and finally reach a stable TSR of 1.95. In the numerical simulation, under 5.5 m/s condition, the turbine is unable to break through the plateau to enter the lift acceleration state falling into the deadband, and the final TSR is 0.65; compared with 5 m/s, the TSR increases by 0.05. When the inlet wind speed increases to 6 m/s, the turbine can generate more torque to make it enter the lift drive state to complete self-starting. The numerical simulation results and experimental findings exhibit discrepancies during the self-starting process, a phenomenon also observed in [Asr et al. \(2016\)](#)'s research. This discrepancy is attributed to factors such as the edge impact of the blades, the wind resistance from the support frames, and the presence of magnetic powder dynamometers. These factors impact the aerodynamic behavior of the turbine, aspects that are neglected in the two-dimensional computational study.

Figure 23 shows the C_t variation of the turbine and single blades during one rotation cycle under 5.5 m/s at $TSR = 0.65$ and 6 m/s at $TSR = 0.7$. For the three-blade turbine, one cycle is 120° . When the turbine operates to 120° , blade 3 rotates to the 0° position of blade 1. Therefore, Fig. 24 and Fig. 25 display contours of static pressure and velocity magnitude at 0° , 30° , 60° , and 90° under 5.5 m/s at $TSR = 0.65$ and 6 m/s at $TSR = 0.7$. Figure 23 (a) shows that a positive torque is generated under both working conditions for azimuthal angles ranging from 0° to 60° and the two conditions exhibit similar trends. In the azimuthal range of 60° to 120° , the 5.5 m/s condition generates massive negative torque, which offsets the positive torque generated by 0° to 60° . The turbine keeps rotating at a constant speed. Compared to the 5.5 m/s condition, the 6 m/s condition generates less negative torque from 60° to 120° . This helps the turbine generate a small amount of positive torque to slowly pass through the deadband. Figure 23(b) shows that the three blades exhibit similar torque coefficient variations at 5.5 m/s or 6 m/s. In the range of 0° to 60° , under 6 m/s condition, the ability to generate positive torque is

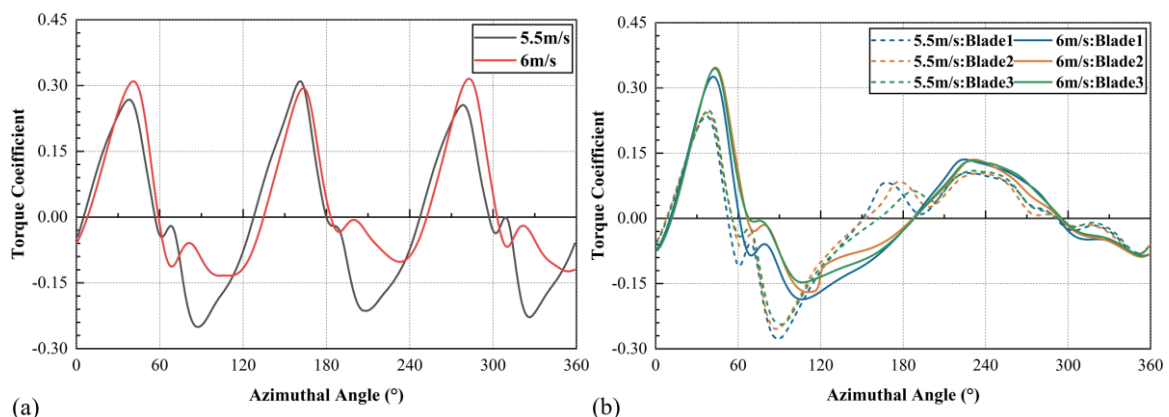
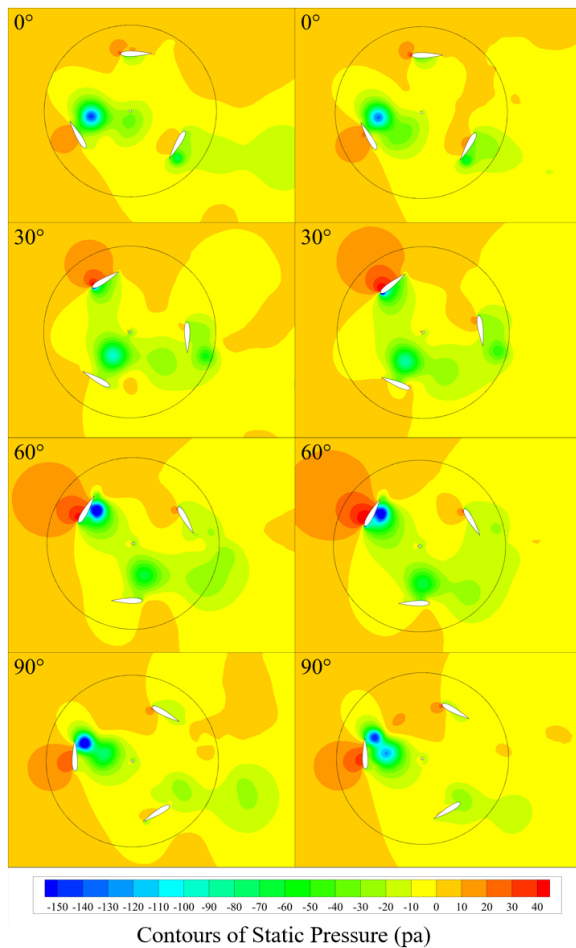
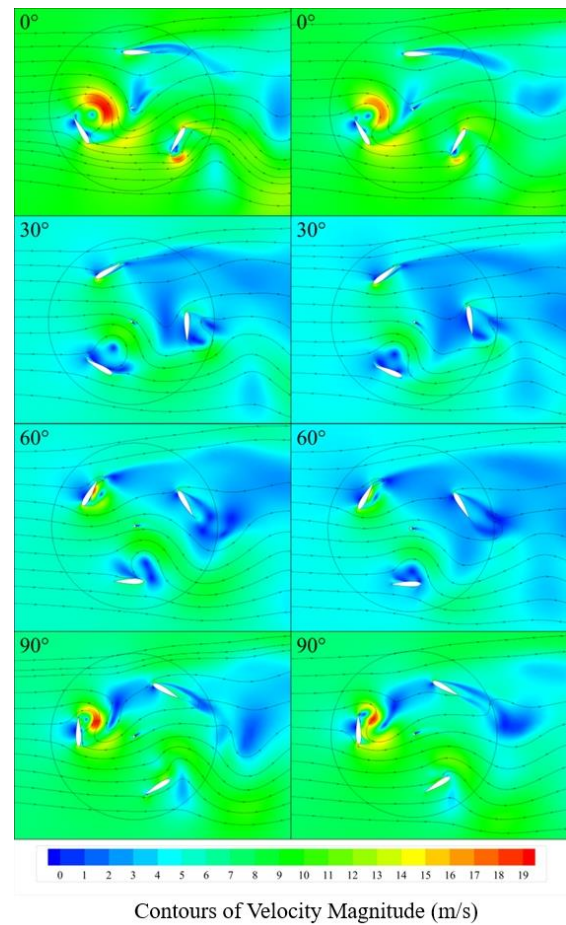


Fig. 23 Variation in the instantaneous torque coefficient with the azimuthal angle for different inlet wind speeds: the turbine (a) and single blades (b)



(a) (b)
Fig. 24 Static pressure contours at azimuthal angles of 0°, 30°, 60° and 90°: 5.5 m/s (a) and 6 m/s (b)

the range of 120° to 180°, under 5.5 m/s condition, positive torque is produced, while at 6 m/s, negative torque is generated. Figure 24 shows the contours of static pressure under two inlet wind speeds. When the turbine is at the 0° azimuthal angle, the pressure distributions exhibit similarities under the two conditions. The positive pressure is observed at the leading edge of blade 1, accompanied by a slight negative pressure on the inner side. This condition leads to the generation of a small negative torque. The trailing edge of blade 2 exhibits negative pressure, generating a large negative torque. When blade 3 interacts with the incoming wind, it induces positive pressure on its inner side and concurrently experiences negative pressure on the outer side, causing the generation of positive torque. Figure 23(b) confirms this phenomenon. Under two wind speed conditions, as the turbine turns counterclockwise, the blade 1 azimuthal angle progresses from 0° to 90°, leading to a relocation of the positive pressure region from the leading edge to the upper edge. However, under the 6 m/s condition, the positive pressure area and value are larger compared to 5.5 m/s. Conversely, the area and value of the negative pressure cause a difference. The contours show that a negative pressure zone is generated under both conditions at the trailing edge of the inner blade. However, the area and value generated at 5.5 m/s are greater than that generated at 6 m/s. Moreover, at 6 m/s, a secondary negative pressure zone emerges in the middle of the inner



(a) (b)
Fig. 25 Velocity magnitude contours at azimuthal angles of 0°, 30°, 60° and 90°: 5.5 m/s (a) and 6 m/s (b)

blade, which decreases negative torque generation. Figure 23(a) shows the torque coefficient has a large difference at 90°. The 6 m/s condition is -0.057, but the 5.5 m/s condition is -0.251.

Figure 25 illustrates the velocity magnitude contours. It is evident that there is a strong resemblance between the two wind speed conditions. This similarity arises because the incoming wind speeds for both conditions are close, and the TSR are also similar. Specifically, the turbine under the 6 m/s condition operates in a plateau state, generating a modest amount of torque, leading to a gradual acceleration. On the other hand, the turbine under the 5.5 m/s condition is in a stable state without additional torque to accelerate the turbine over the plateau. Consequently, the velocity magnitude contours and streamlines exhibit a high degree of similarity between the two conditions.

5. CONCLUSIONS

The self-starting performance evaluation of VAWTs can be divided into static start-up performance and dynamic start-up performance. Traditional methods relying on the static torque coefficient or self-starting time exhibit limitations. Based on the observed power performance characteristics and the variations in angular acceleration, including the first derivative of angular

acceleration, for the very first time, "the minimum 1st derivative of angular acceleration in the lift acceleration state" is proposed to be the indicator of self-starting completion. The self-starting performance of three NACA airfoil wind turbines is investigated. The effects of the static evaluation method on the dynamic start-up process and the effects of airfoils, pitch angles, and inlet wind speeds on the dynamic start-up process are studied. Our main conclusions are as follows:

1. An initial azimuthal angle with a low static torque coefficient may cause the turbine to be stationary and unable to rotate. A high static torque coefficient can ensure that the turbine can rotate at the beginning. However, the subsequent self-starting time is independent of the static torque coefficient.

2. The effects of pitch angles and airfoils are investigated. Increasing the pitch angle enhances the self-starting performance. For the NACA2418 airfoil turbine, the self-starting times for pitch angles of 10° and 5° are reduced by 20% and 12%, respectively, compared to that for 0°. The negative torque contribution of drag is distinct. For the NACA0018 airfoil turbine, pitch angles of 0° and 5° fail to self-start, with only the 10° pitch angle completing the self-starting process.

3. The airfoil NACA0018 airfoil turbine failed to complete self-starting; the maximum C_p reached 0.156 with assisted starting. The self-starting performance of the NACA2418 airfoil turbine is better than those of the other two airfoils, and its C_p is slightly lower than that of the NACA0018 airfoil; this result shows the best comprehensive performance.

4. The analysis of the minimum self-starting wind speed of the NACA0018 airfoil turbine shows that the self-starting wind speed is between 5.5 m/s and 6 m/s. At 0° to 60° azimuthal angles, positive torque is generated under inlet wind speeds of 5.5 m/s and 6 m/s. At 60° to 120° azimuthal angles, the 5.5 m/s condition generates massive negative torque, which offsets the positive torque generated by 0° to 60°. Thus, the turbine is in a stable rotational state at 5.5 m/s, while at 6 m/s and can overcome the plateau state to complete the self-starting process.

ACKNOWLEDGMENTS

The National Natural Science Foundation of China (No. 61802347) has provided financial support for this study.

CONFLICT OF INTEREST

The authors assert that they do not have any identifiable conflicting financial interests or personal relationships that could be perceived as influencing the findings presented in this paper.

AUTHOR CONTRIBUTIONS

Zhang Xu: Conceptualization, Methodology; Xiuchen Dong: Data curation, Writing-original draft, Writing-review & editing. **Kairong Li:** Formal analysis, Visualization, **Qianwei Zhou:** Funding acquisition, Supervision. **Yunhua Zhao:** Project administration,

Validation.

DATA AVAILABILITY

The corresponding author will provide the data supporting the results upon reasonable request.

REFERENCES

- Al-Obaidi, A. (2018). *Experimental and numerical investigations on the cavitation phenomenon in a centrifugal pump* [thesis or dissertation, University of Huddersfield].
- Al-Obaidi, A., Khalaf, H., & Alhamid, J. (2023a). *Investigation of the influence of varying operation configurations on flow behaviors characteristics and hydraulic axial-flow pump performance*. Proceedings of the 4th International Conference on Science Education in The Industrial Revolution 4.0, ICONSEIR 2022, November 24th, 2022, Medan, Indonesia.
- Al-Obaidi, A., Khalaf, H., & Alhamid, J. (2023b). *Investigation on the characteristics of internal flow within three-dimensional axial pump based on different flow conditions*. Proceedings of the 4th International Conference on Science Education in The Industrial Revolution 4.0, ICONSEIR 2022, November 24th, 2022, Medan, Indonesia.
- Al-Obaidi, A. R. (2019). Investigation of effect of pump rotational speed on performance and detection of cavitation within a centrifugal pump using vibration analysis. *Heliyon*, 5(6).
- Al-Obaidi, A. R. (2023a). Effect of different guide vane configurations on flow field investigation and performances of an axial pump based on CFD analysis and vibration investigation. *Experimental Techniques*, 1-20. <https://doi.org/10.1007/s40799-023-00641-5>
- Al-Obaidi, A. R. (2023b). Experimental diagnostic of cavitation flow in the centrifugal pump under various impeller speeds based on acoustic analysis method. *Archives of Acoustics*, 48(2), 159-170. <https://doi.org/10.24425/aoa.2023.145234>
- Al-Obaidi, A. R., & Alhamid, J. (2023). Investigation of the Main flow characteristics mechanism and flow dynamics within an axial flow pump based on different transient load conditions. *Iranian Journal of Science and Technology-Transactions of Mechanical Engineering*, 1-19. <https://doi.org/10.1007/s40997-022-00586-x>
- Al-Obaidi, A. R., & Qubian, A. (2022). Effect of outlet impeller diameter on performance prediction of centrifugal pump under single-phase and cavitation flow conditions. *International Journal of Nonlinear Sciences and Numerical Simulation*, 23(7-8), 1203-1229. <https://doi.org/10.1515/ijnsns-2020-0119>
- Alam, F., & Golde, S. (2013). *An aerodynamic study of a micro scale vertical axis wind turbine*. 5th Bsmc International Conference on Thermal Engineering, 56, 568-572. <https://doi.org/10.1016/j.proeng.2013.03.161>

- Almohammadi, K. M., Ingham, D. B., Ma, L., & Pourkashan, M. (2013). Computational fluid dynamics (CFD) mesh independency techniques for a straight blade vertical axis wind turbine. *Energy*, 58, 483-493. <https://doi.org/10.1016/j.energy.2013.06.012>
- Ansys, I. (2018). *ANSYS fluent user's guide, release 19.0*. ANSYS Inc, Canonsburg.
- Arab, A., Javadi, M., Anbarsooz, M., & Moghiman, M. (2017). A numerical study on the aerodynamic performance and the self-starting characteristics of a Darrieus wind turbine considering its moment of inertia. *Renewable Energy*, 107, 298-311. <https://doi.org/10.1016/j.renene.2017.02.013>
- Arpino, F., Scungio, M., & Cortellessa, G. (2018). Numerical performance assessment of an innovative Darrieus-style vertical axis wind turbine with auxiliary straight blades. *Energy Conversion and Management*, 171, 769-777. <https://doi.org/10.1016/j.enconman.2018.06.028>
- Asr, M. T., Nezhad, E. Z., Mustapha, F., & Wiriadidjaja, S. (2016). Study on start-up characteristics of H-Darrieus vertical axis wind turbines comprising NACA 4-digit series blade airfoils. *Energy*, 112, 528-537. <https://doi.org/10.1016/j.energy.2016.06.059>
- Baker, J. (1983). Features to aid or enable self starting of fixed pitch low solidity vertical axis wind turbines. *Journal of Wind Engineering and Industrial Aerodynamics*, 15(1-3), 369-380.
- Balduzzi, F., Bianchini, A., Maleci, R., Ferrara, G., & Ferrari, L. (2016). Critical issues in the CFD simulation of Darrieus wind turbines. *Renewable Energy*, 85, 419-435. <https://doi.org/10.1016/j.renene.2015.06.048>
- Bangga, G., Hutani, S., & Heramarwan, H. (2021). The effects of airfoil thickness on dynamic stall characteristics of high-solidity vertical axis wind turbines. *Advanced Theory and Simulations*, 4(6), 2000204. <https://doi.org/ARTN200020410.1002/adts.202000204>
- Battisti, L., Benini, E., Brighenti, A., Dell'Anna, S., & Castelli, M. R. (2018). Small wind turbine effectiveness in the urban environment. *Renewable Energy*, 129, 102-113. <https://doi.org/10.1016/j.renene.2018.05.062>
- Bhuyan, S., & Biswas, A. (2014). Investigations on self-starting and performance characteristics of simple H and hybrid H-Savonius vertical axis wind rotors. *Energy Conversion and Management*, 87, 859-867. <https://doi.org/10.1016/j.enconman.2014.07.056>
- Celik, Y., Ingham, D., Ma, L., & Pourkashanian, M. (2022). Design and aerodynamic performance analyses of the self-starting H-type VAWT having J-shaped aerofoils considering various design parameters using CFD. *Energy*, 251, 123881. <https://doi.org/ARTN12388110.1016/j.energy.2022.123881>
- Celik, Y., Ma, L., Ingham, D., & Pourkashanian, M. (2020). Aerodynamic investigation of the start-up process of H-type vertical axis wind turbines using CFD. *Journal of Wind Engineering and Industrial Aerodynamics*, 204, 104252. <https://doi.org/ARTN10425210.1016/j.jweia.2020.104252>
- Chang, T. L., Tsai, S. F., & Chen, C. L. (2021). Optimal design of novel blade profile for savonius wind turbines. *Energies*, 14(12).
- Ebert, P. R., & Wood, D. H. (1997). Observations of the starting behaviour of a small horizontal axis wind turbine. *Renewable Energy*, 12(3), 245-257. [https://doi.org/10.1016/s0960-1481\(97\)00035-9](https://doi.org/10.1016/s0960-1481(97)00035-9)
- GWEC, G. W. E. C. (2023). Global Wind Report 2023. In: GWEC.
- Hand, B., & Cashman, A. (2020). A review on the historical development of the lift-type vertical axis wind turbine: From onshore to offshore floating application. *Sustainable Energy Technologies and Assessments*, 38, 100646. <https://doi.org/ARTN10064610.1016/j.seta.2020.100646>
- Hashem, I., & Mohamed, M. H. (2018). Aerodynamic performance enhancements of H-rotor Darrieus wind turbine. *Energy*, 142, 531-545. <https://doi.org/10.1016/j.energy.2017.10.036>
- Hill, N., Dominy, R., Ingram, G., & Dominy, J. (2008). Darrieus turbines: The physics of self-starting. *Proceedings of the Institution of Mechanical Engineers, Part A: Journal of Power and Energy*, 223(1), 21-29. <https://doi.org/10.1243/09576509jpe615>
- Howell, R., Qin, N., Edwards, J., & Durrani, N. (2010). Wind tunnel and numerical study of a small vertical axis wind turbine. *Renewable Energy*, 35(2), 412-422. <https://doi.org/10.1016/j.renene.2009.07.025>
- Islam, M. R., Mekhilef, S., & Saidur, R. (2013). Progress and recent trends of wind energy technology. *Renewable & Sustainable Energy Reviews*, 21, 456-468. <https://doi.org/10.1016/j.rser.2013.01.007>
- Kaya, M. N., Kose, F., Ingham, D., Ma, L., & Pourkashanian, M. (2018). Aerodynamic performance of a horizontal axis wind turbine with forward and backward swept blades. *Journal of Wind Engineering and Industrial Aerodynamics*, 176, 166-173. <https://doi.org/10.1016/j.jweia.2018.03.023>
- Kumar, R., Raahemifar, K., & Fung, A. S. (2018). A critical review of vertical axis wind turbines for urban applications. *Renewable & Sustainable Energy Reviews*, 89, 281-291. <https://doi.org/10.1016/j.rser.2018.03.033>
- Li, Q. A., Maeda, T., Kamada, Y., Murata, J., Shimizu, K., Ogasawara, T., . . . Kasuya, T. (2016). Effect of solidity on aerodynamic forces around straight-bladed vertical axis wind turbine by wind tunnel experiments (depending on number of blades). *Renewable Energy*, 96, 928-939. <https://doi.org/10.1016/j.renene.2016.05.054>
- Li, Q. A., Maeda, T., Kamada, Y., Shimizu, K., Ogasawara, T., Nakai, A., & Kasuya, T. (2017). Effect of rotor

- aspect ratio and solidity on a straight-bladed vertical axis wind turbine in three-dimensional analysis by the panel method. *Energy*, *121*, 1-9. <https://doi.org/10.1016/j.energy.2016.12.112>
- Li, Y., Zhao, S. Y., Qu, C. M., Feng, F., & Kotaro, T. (2019). effects of offset blade on aerodynamic characteristics of small-scale vertical axis wind turbine. *Journal of Thermal Science*, *28*(2), 326-339. <https://doi.org/10.1007/s11630-018-1058-4>
- Li, Y., Zhao, S. Y., Qu, C. M., Tong, G. Q., Feng, F., Zhao, B., & Kotaro, T. (2020). Aerodynamic characteristics of straight-bladed vertical axis wind turbine with a curved-outline wind gathering device. *Energy Conversion and Management*, *203*, 112249. <https://doi.org/ARTN11224910.1016/j.enconman.2019.112249>
- Liu, J., Lin, H., & Zhang, J. (2019). Review on the technical perspectives and commercial viability of vertical axis wind turbines. *Ocean Engineering*, *182*, 608-626. <https://doi.org/10.1016/j.oceaneng.2019.04.086>
- Lunt, P. (2005). *An aerodynamic model for a vertical-axis wind turbine*. MEng Project Report, School of Engineering, University of Durham, UK.
- Maalouly, M., Souaiby, M., ElCheikh, A., Issa, J. S., & Elkhoury, M. (2022). Transient analysis of H-type Vertical Axis Wind Turbines using CFD. *Energy Reports*, *8*, 4570-4588. <https://doi.org/10.1016/j.egy.2022.03.136>
- Mohamed, M. H., Dessoky, A., & Alqurashi, F. (2019). Blade shape effect on the behavior of the H-rotor Darrieus wind turbine: Performance investigation and force analysis. *Energy*, *179*, 1217-1234. <https://doi.org/10.1016/j.energy.2019.05.069>
- Mohamed, O. S., Ibrahim, A. A., Etman, A. K., Abdelfatah, A. A., & Elbaz, A. M. R. (2020). Numerical investigation of Darrieus wind turbine with slotted airfoil blades. *Energy Conversion and Management: X*, *5*, 100026. <https://doi.org/10.1016/j.ecmx.2019.100026>
- Nobile, R., Vandati, M., Barlow, J. F., & Mewburn-Crook, A. (2014). Unsteady flow simulation of a vertical axis augmented wind turbine: A two-dimensional study. *Journal of Wind Engineering and Industrial Aerodynamics*, *125*, 168-179. <https://doi.org/10.1016/j.jweia.2013.12.005>
- Rezaeiha, A., Montazeri, H., & Blocken, B. (2018a). Characterization of aerodynamic performance of vertical axis wind turbines: Impact of operational parameters. *Energy Conversion and Management*, *169*, 45-77. <https://doi.org/10.1016/j.enconman.2018.05.042>
- Rezaeiha, A., Montazeri, H., & Blocken, B. (2018b). Towards accurate CFD simulations of vertical axis wind turbines at different tip speed ratios and solidities: Guidelines for azimuthal increment, domain size and convergence. *Energy Conversion and Management*, *156*, 301-316. <https://doi.org/10.1016/j.enconman.2017.11.026>
- Roy, S., & Saha, U. K. (2014). An adapted blockage factor correlation approach in wind tunnel experiments of a Savonius-style wind turbine. *Energy Conversion and Management*, *86*, 418-427. <https://doi.org/https://doi.org/10.1016/j.enconman.2014.05.039>
- Sheldahl, R. E., Blackwell, B. F., & Feltz, L. V. (1978). Wind tunnel performance data for two- and three-bucket Savonius rotors. *Journal of Energy*, *2*(3), 160-164. <https://doi.org/10.2514/3.47966>
- Singh, M. A., Biswas, A., & Misra, R. D. (2015). Investigation of self-starting and high rotor solidity on the performance of a three S1210 blade H-type Darrieus rotor. *Renewable Energy*, *76*, 381-387. <https://doi.org/10.1016/j.renene.2014.11.027>
- Sobhani, E., Ghaffari, M., & Maghrebi, M. J. (2017). Numerical investigation of dimple effects on darrieus vertical axis wind turbine. *Energy*, *133*, 231-241. <https://doi.org/10.1016/j.energy.2017.05.105>
- Su, H., Dou, B. Z., Qu, T. M., Zeng, P., & Lei, L. P. (2020). Experimental investigation of a novel vertical axis wind turbine with pitching and self-starting function. *Energy Conversion and Management*, *217*, 113012. <https://doi.org/ARTN11301210.1016/j.enconman.2020.113012>
- Su, J., Lei, H., Zhou, D., Han, Z. L., Bao, Y., & Zhu, H. B. (2019). Aerodynamic noise assessment for a vertical axis wind turbine using Improved Delayed Detached Eddy Simulation. *Renewable Energy*, *141*, 559-569. <https://doi.org/10.1016/j.renene.2019.04.038>
- Sun, X. J., Zhu, J. Y., Hanif, A., Li, Z. J., & Sun, G. X. (2020). Effects of blade shape and its corresponding moment of inertia on self-starting and power extraction performance of the novel bowl-shaped floating straight-bladed vertical axis wind turbine. *Sustainable Energy Technologies and Assessments*, *38*, 100648. <https://doi.org/ARTN10064810.1016/j.seta.2020.100648>
- Tong, W. (2010). *Wind power generation and wind turbine design*. WIT press.
- Twidell, J. (2021). *Renewable energy resources*. Routledge.
- Wong, K. H., Chong, W. T., Sukiman, N. L., Shiah, Y. C., Poh, S. C., Sopian, K., & Wang, W. C. (2018). Experimental and simulation investigation into the effects of a flat plate deflector on vertical axis wind turbine. *Energy Conversion and Management*, *160*, 109-125. <https://doi.org/10.1016/j.enconman.2018.01.029>
- Worasinchai, S., Ingram, G. L., & Dominy, R. G. (2012). *The physics of h-darrieus turbines self-starting capability: flapping-wing perspective*. ASME Turbo Expo 2012: Turbine Technical Conference and Exposition.
- Worasinchai, S., Ingram, G. L., & Dominy, R. G. (2016). The physics of H-Darrieus turbine starting behavior. *Journal of Engineering for Gas Turbines and Power-Transactions of the Asme*, *138*(6), 062605. <https://doi.org/ArtN06260510.1115/1.4031870>

Zhu, H. T., Hao, W. X., Li, C., Luo, S., Liu, Q. S., & Gao, C. (2021). Effect of geometric parameters of Gurney flap on performance enhancement of straight-bladed vertical axis wind turbine. *Renewable Energy*, 165, 464-480.
<https://doi.org/10.1016/j.renene.2020.11.027>

Zhu, J. Y., Huang, H. L., & Shen, H. (2015). Self-starting aerodynamics analysis of vertical axis wind turbine. *Advances in Mechanical Engineering*, 7(12), 1687814015620968. <https://doi.org/Artn168781401562096810.1177/1687814015620968>